Supplemental Material to "Optical Magnetism and Huygens' Surfaces in Arrays of Atoms Induced by Cooperative Responses"

K. E. Ballantine and J. Ruostekoski
Department of Physics, Lancaster University, Lancaster, LA1 4YB, United Kingdom
(Dated: August 14, 2020)

In this supplemental material we briefly recap the basic relations for the electrodynamics of light and atoms, and further illustrate the role of collective excitations for the example of synthesizing optical magnetism. We provide some additional details of the spherical harmonics used to decompose the far-field radiation and the scattered light and excitations of the Huygens' surface. We show an additional demonstration of the Huygens' surface in the generation of a single orbital angular momentum state with $\hbar$ angular momentum per photon.

SI. ELECTRODYNAMICS OF LIGHT AND ATOMS

SI.A. Equations of motion

In the main section we characterize the optical response of both the unit-cell and the many-atom array by writing the equations of motion as $\dot{\mathbf{b}} = i\mathcal{H}\mathbf{b} + \mathbf{F}$ where $\mathbf{b}$ is the vector of polarization amplitudes $\mathcal{P}_\sigma^{(j)}$ and $\mathbf{F}$ represents the external driving by the incident light. To see the origin of these equations we note that in the limit of low light intensity, the polarization amplitudes obey [S1, S2]

$$\frac{d}{dt}\mathcal{P}_\mu^{(j)} = \left(i\Delta_\mu^{(j)} - \gamma\right)\mathcal{P}_\mu^{(j)} + i\frac{\xi}{\mathcal{D}}\hat{\mathbf{e}}_\mu^* \cdot \epsilon_0 \mathbf{E}_{\rm ext}(\mathbf{r}_j), \quad \text{(S1)}$$

where $\xi = 6\pi\gamma/k^3$, the single atom linewidth is $\gamma = \mathcal{D}^2k^3/6\pi\hbar\epsilon_0$, and $\Delta_\mu^{(j)} = \omega - \omega_\mu^{(j)}$ are the the detunings of the $m = \mu$ level of atom j from resonance. The light and atomic field amplitudes here refer to the slowly varying positive frequency components, where the rapid oscillations $\exp(-i\omega t)$ at the laser frequency have been factored out. Each amplitude $\mathcal{P}_\mu^{(j)}$ at position $\mathbf{r}_j$ is driven by the field,

$$\mathbf{E}_{\rm ext}(\mathbf{r}_j) = \boldsymbol{\mathcal{E}}(\mathbf{r}_j) + \sum_{l\neq j}\mathbf{E}_s^{(l)}(\mathbf{r}_j), \quad \text{(S2)}$$

which consists of the the incident field $\boldsymbol{\mathcal{E}}(\mathbf{r})$ and the scattered field $\epsilon_0\mathbf{E}_s^{(l)}(\mathbf{r}) = \mathsf{G}(\mathbf{r}-\mathbf{r}_l)\mathbf{d}_l$ from the dipole moment $\mathbf{d}_l$ of each other atom l. The scattered field expression equals the usual positive-frequency component of the electric field from a monochromatic dipole $\mathbf{d}$, given that the dipole resides at the origin and the field is observed at $\mathbf{r}$ [S3]:

$$\mathsf{G}(\mathbf{r})\mathbf{d} = \frac{1}{4\pi\epsilon_0}\big\{k^2(\hat{\mathbf{n}}\times\mathbf{d})\times\hat{\mathbf{n}}\frac{e^{ikr}}{r} + [3\hat{\mathbf{n}}(\hat{\mathbf{n}}\cdot\mathbf{d}) - \mathbf{d}]\big(\frac{1}{r^3} - \frac{ik}{r^2}\big)e^{ikr}\big\} - \frac{\mathbf{d}}{3\epsilon_0}\delta(\mathbf{r}), \quad \text{(S3)}$$

with $\hat{\mathbf{n}} = \mathbf{r}/r$ and $k = \omega/c$.

Inserting Eq. (S2) into Eq. (S1), with the dipole moment expressed in terms of the polarization as $\mathbf{d}_j = \mathcal{D}\sum_\mu \hat{\mathbf{e}}_\mu\mathcal{P}_\mu^{(j)}$, gives

$$\frac{d}{dt}\mathcal{P}_\mu^{(j)} = \left(i\Delta_\mu^{(j)} - \gamma\right)\mathcal{P}_\mu^{(j)} + i\xi\sum_{l\neq j}\mathcal{G}_{\mu\nu}^{(jl)}\mathcal{P}_\nu^{(l)} + i\frac{\xi}{\mathcal{D}}\hat{\mathbf{e}}_\mu^*\cdot\epsilon_0\boldsymbol{\mathcal{E}}(\mathbf{r}_j), \quad \text{(S4)}$$

with $\mathcal{G}_{\mu\nu}^{(jl)} = \hat{\mathbf{e}}_\mu^*\cdot\mathsf{G}(\mathbf{r}_j - \mathbf{r}_l)\hat{\mathbf{e}}_\nu$. The linear equations of motion can then be written in matrix form as above.

This equation also describes the decay of a single photon excitation. The full quantum dynamics of the atomic system for a given initial excitation and in the absence of a driving laser follows from the quantum master equation for the many-atom density matrix ρ,

$$\dot{\rho} = i\sum_{j,\nu}\Delta_\nu\left[\hat{\sigma}_{j\nu}^+\hat{\sigma}_{j\nu}^-,\rho\right] + i\sum_{jl\nu\mu(l\neq j)}\Omega_{\nu\mu}^{(jl)}\left[\hat{\sigma}_{j\nu}^+\hat{\sigma}_{l\mu}^-,\rho\right] + \sum_{jl\nu\mu}\gamma_{\nu\mu}^{(jl)}\left(2\hat{\sigma}_{l\mu}^-\rho\hat{\sigma}_{j\nu}^+ - \hat{\sigma}_{j\nu}^+\hat{\sigma}_{l\mu}^-\rho - \rho\hat{\sigma}_{j\nu}^+\hat{\sigma}_{l\mu}^-\right), \quad \text{(S5)}$$

where $\hat{\sigma}_{j\nu}^+ = (\hat{\sigma}_{j\nu}^-)^\dagger = |e_{j\nu}\rangle\langle g_j|$ is the raising operator to the excited state ν on atom j. The diagonal terms of the dissipative matrix are $\gamma_{\nu\nu}^{(jj)} = \gamma$, while the off-diagonal elements of the dissipation and interaction terms are given by the real and imaginary parts of

$$\Omega_{\nu\mu}^{(jl)} + i\gamma_{\nu\mu}^{(jl)} = \xi\mathcal{G}_{\nu\mu}^{(jl)}. \quad \text{(S6)}$$

Restricting to the subspace of at most a single excitation, and assuming a pure initial state, the density matrix splits into one excitation and zero excitation parts,

$$\rho = |\psi\rangle\langle\psi| + p_g|G\rangle\langle G|, \quad \text{(S7)}$$

where $|\psi\rangle$ represents a single excitation and can be expanded over the atomic sites,

$$|\psi\rangle = \sum_{j,\nu}\mathcal{P}_\nu^{(j)}(t)\,\hat{\sigma}_{j\nu}^+|G\rangle, \quad \text{(S8)}$$

and $|G\rangle$ is the ground state. Regarding single-particle expectation values, the dynamics can equally be described by the evolution of a vector $\mathbf{b}$ of these amplitudes $\mathcal{P}_\nu^{(j)}$ [S4], which obey the same equations as the classical polarization in the absence of drive, $\dot{\mathbf{b}} = i\mathcal{H}\mathbf{b}$.

SI.B. Collective excitation eigenmodes

In both the case of the evolution of a single atomic excitation and the case of driven classical polarization, the optical response of the lattice is then characterized by the eigenvectors $\mathbf{v}_n$ and eigenvalues $\delta_n + i\upsilon_n$, of the evolution matrix $\mathcal{H}$ [S5]. While the eigenmodes are not orthogonal, due to $\mathcal{H}$ being non-Hermitian, we find in our numerics that they always form a basis. Hence, the state at a time t can be expanded in this basis $\mathbf{b}(t) = \sum_n c_n \mathbf{v}_n$. We define the quantity

$$L_j = \frac{|\mathbf{v}_j^T \mathbf{b}(t)|^2}{\sum_i |\mathbf{v}_i^T \mathbf{b}(t)|^2}, \tag{S9}$$

as a measure of the relative occupation of each collective mode [S6].

SII. EIGENMODES OF A SINGLE UNIT-CELL

We display in Fig. S1 the excitation eigenmodes of a single isolated unit-cell of a planar array used to generate optically active magnetism [Fig. 1(a) in the main section]. Each unit-cell consists of four atoms and therefore 12 eigenmodes of which three are degenerate with some of the other modes and are obtained by trivial symmetry transformations of the dipole orientations. The properties of the eigenmodes are listed in Table 1 of the main section.

SIII. COUPLING TO COLLECTIVE MAGNETIC MODE

The excitation of a collective mode consisting of magnetic dipoles in a planar array via the coupling between electric dipole eigenmodes (EDM) and magnetic dipole eigenmodes (MDM) is described by a two-mode model [Eq. (2) in the main section]. The incident field with the polarization $(\hat{\mathbf{e}}_y + \hat{\mathbf{e}}_z)/\sqrt{2}$ drives the EDM. The EDM in the y and z direction are clearly degenerate due to symmetry, and so the excited symmetric combination is also an eigenmode, with amplitude $\mathcal{P}_e$. When all the electronically excited levels are degenerate, this mode evolves independently of the MDM of amplitude $\mathcal{P}_m$ which is not excited.

When the level shifts are not equal ($\Delta_{\pm,0}^{(j)} \neq 0$), $\mathcal{P}_e$ and $\mathcal{P}_m$ no longer describe eigenmodes, and these are coupled together (as generally could the other eigenmodes of the $\Delta_{\pm,0}^{(j)} = 0$ system). As shown in Fig. S1, the array of

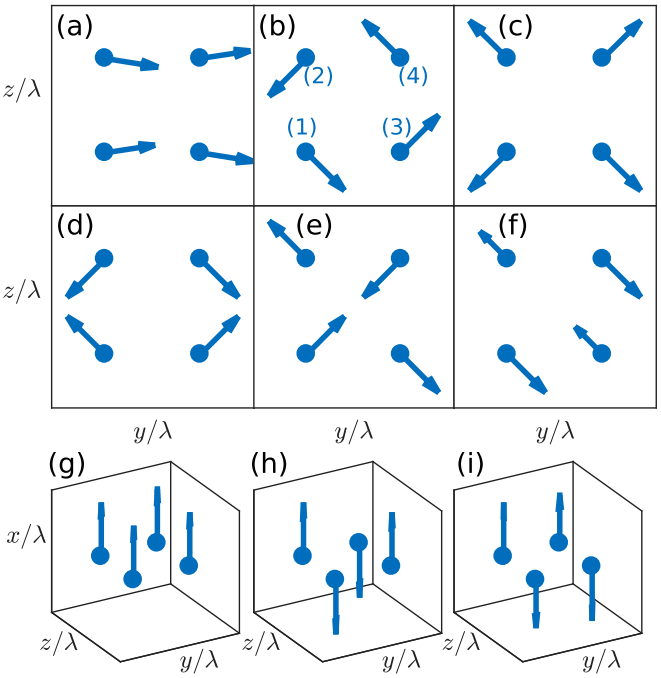

FIG. S1. The orientation of the atomic dipoles for the eigenmodes of an isolated square unit-cell, with the same ordering as Table 1 of the main section, for the spacing $a = 0.15\lambda$. Top and middle row: in-plane modes consisting of (a) electric dipole, (b) magnetic dipole ($n = 4$), (c-e) electric quadrupole modes, and (f) mixed multipole character. Bottom row: modes with x polarization consisting of (a) Electric dipole and (b-c) mixed multipole. Note the modes shown in (a), (f), and (i) are each doubly degenerate due to lattice symmetry. The ordering of the sites given in the text for the atomic level shifts is illustrated in (b).

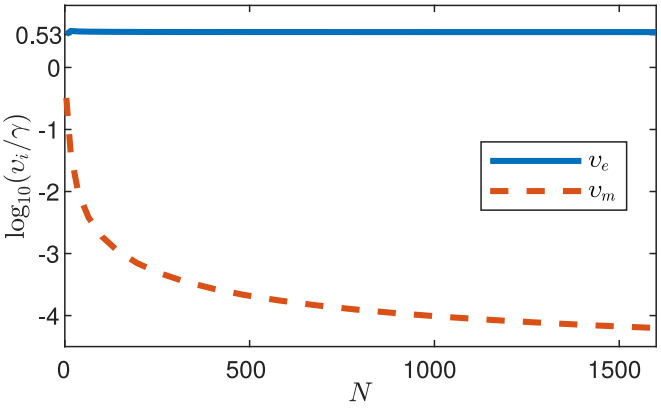

FIG. S2. The collective linewidths υ_e and υ_m of the electric and magnetic dipole modes as a function of total atom number N for a lattice with $a = 0.15\lambda$ and $d = 0.5\lambda$. While the linewidth of the magnetic mode depends strongly on N, the linewidth of the electric mode is almost constant, starting at $\upsilon_m = 3.4$ for a single unit-cell and rising to 3.7 at $N = 1600$.

atoms in the yz plane [Fig. 1(a) in the main section] has two separate families of modes, those with polarization in the x direction out of the plane and those with polarizations in the plane. To avoid coupling the drive to those out of plane modes we choose $\Delta_+^{(j)} = \Delta_-^{(j)}$ on each atom. Then, to couple the EDM to the alternating phases of the y and z components of the MDM, we choose the remaining level shifts to have similarly alternating signs:

$$(\delta^{(\pm)}_{(4j+1)}, \delta^{(\pm)}_{(4j+2)}, \delta^{(\pm)}_{(4j+3)}, \delta^{(\pm)}_{(4j+4)}) = \delta(2, 0, 2, 0), \quad \text{(S10a)}$$

$$(\delta^{(0)}_{(4j+1)}, \delta^{(0)}_{(4j+2)}, \delta^{(0)}_{(4j+3)}, \delta^{(0)}_{(4j+4)}) = \delta(0, 0, 2, 2), \quad \text{(S10b)}$$

where the ordering of the atoms is shown in Fig. S1(b).

The periodic variation of the level shifts can be produced by the ac Stark shift of an external standing-wave laser with the intensity varying along the principal axes of the array, such that the levels $m = \pm 1$ are shifted using an intensity variation along the z direction and the shift of the $m = 0$ state with the intensity variation along the y direction. In the both cases the intensity maxima are then separated by the distance d between the adjacent unit-cells. Suitable transitions could be found, e.g., with Sr or Yb. For example, for the $^3P_0 \to {}^3D_1$ transition of ^{88}Sr the resonance wavelength $\lambda \simeq 2.6\mu$m and the linewidth 2.9×10^5/s [S7]. For the case of optical lattices the periodicity of the sinusoidal potential for the same transition with a magic wavelength may be chosen as 206.4nm and can also be modified to achieve the right periodicity by tilting the propagation direction of the lasers forming the lattice. Alternatively, atoms in different hyperfine states could occupy different lattice sites [S8], with the associated description of the atom-light dynamics [S2, S5], or the trapping potential strength for tweezers could possibly be spatially varied.

With this choice of level shifts given by Eq. (S10) we obtain [Eq. (2) in the main section],

$$\partial_t \mathcal{P}_e^{(j)} = (i\delta_e + i\Delta - \upsilon_e)\mathcal{P}_e^{(j)} + \delta \mathcal{P}_m^{(j)} + f, \quad \text{(S11a)}$$

$$\partial_t \mathcal{P}_m^{(j)} = (i\delta_m + i\Delta - \upsilon_m)\mathcal{P}_m^{(j)} + \delta \mathcal{P}_e^{(j)}. \quad \text{(S11b)}$$

The effective dynamics of Eqs. (S11) can represent both a single unit-cell in isolation and the entire array of multiple unit-cells, but the collective resonance line shifts and linewidths of the EDM and MDM, $\delta_{e,m}$ and $\upsilon_{e,m}$, respectively, can considerably differ in the two cases, and generally vary with the number of unit-cells (Fig. S2). The driving field is denoted by $f = i\xi\epsilon_0\mathcal{E}_0/\mathcal{D}$. The alternating signs of $\Delta^{(j)}_{-,0}$ mean there is no coupling to other unit-cell eigenmodes with different symmetries.

The steady state of Eqs. (S11) is easily solved and we find the ratio of the MDM and EDM amplitudes to be

$$\left|\frac{\mathcal{P}_m}{\mathcal{P}_e}\right| = \left|\frac{\delta}{i\delta_m + i\Delta - \upsilon_m}\right|. \quad \text{(S12)}$$

On resonance, $\Delta = -\delta_m$, the ratio of amplitudes is determined by the collective linewidth υ_m. As shown in Fig. S2 the linewidth of the MDM rapidly narrows as a function of the array size and becomes strongly subradiant. It is this collective resonance narrowing which allows the amplitude of the MDM to become large compared with the EDM amplitude, even for relatively small detuning strength δ.

Equations (S11) are similar to those describing the electromagnetically-induced transparency [S9] of 'dark' and 'bright' states of noninteracting atoms in which case the atom population can be trapped in the dark state. In the present case, the dark state is represented by a collective eigenmode, resulting from the resonant dipole-dipole interactions. It is this collective subradiant nature of the mode that drives the excitation into the MDM.

SIV. SPHERICAL HARMONICS

The multipole moments of the lattice unit-cells are characterized from the far-field radiation by decomposing the field in terms of vector spherical harmonics [S3] [Eq. (1) in the main section]. The vector spherical harmonics are defined in terms of the ordinary spherical harmonics $Y_{lm}(\theta, \phi)$ as $\mathbf{\Psi}_{lm} = r\nabla Y_{lm}$ and $\mathbf{\Phi}_{lm} = \mathbf{r} \times \nabla Y_{lm}$ where $\mathbf{r}$ is the vector from the origin to the observation point, θ is the polar angle with the x axis, and ϕ is the azimuthal angle from the y axis in the yz plane. They are orthogonal; $\int \mathbf{\Psi}^*_{lm}\mathbf{\Psi}_{l'm'}\mathrm{d}\Omega = \int \mathbf{\Phi}^*_{lm}\mathbf{\Phi}_{l'm'}\mathrm{d}\Omega = l(l+1)\delta_{ll'}\delta_{mm'}$, $\int \mathbf{\Psi}^*_{lm}\mathbf{\Phi}_{l'm'}\mathrm{d}\Omega = 0$, and so the coefficients α can be found by projecting onto the corresponding vector harmonic.

SV. HUYGENS' SURFACE

For analyzing the properties of the Huygens' surface, the contributions of the both incident and scattered light are included. The scattered light can be calculated by summing up all the light scattered from all the atoms in the array. We have verified that the transmission of light at distances $\lambda \lesssim \xi \ll \sqrt{\mathcal{A}}$ from a planar array of uniform excitations, where $\mathcal{A}$ denotes the area of the array, can also be estimated by [S10–S13]

$$\epsilon_0 \mathbf{E} = \mathcal{E}_0 \hat{\mathbf{e}}_y e^{ik\xi} + \frac{ik}{2\mathcal{A}} \sum_k \left[\mathbf{d}_k - \hat{\mathbf{e}}_x \cdot \mathbf{d}_k \hat{\mathbf{e}}_x\right] e^{i(\xi - x_k)}, \quad \text{(S13)}$$

where the second term denotes the scattered field $\mathbf{E}_S$ and the first term is the incident field. This expression has been used together with the microscopic calculation to analyze Huygens' surface, e.g., in Fig. 3 in the main section.

In Fig. S3 we show the magnitude and the phase of the total transmitted field, and also the contribution of the scattered field alone. Fig. S3(b) shows that while the phase of the scattered field covers a range of π, the total field has a full range of 2π. The contribution from

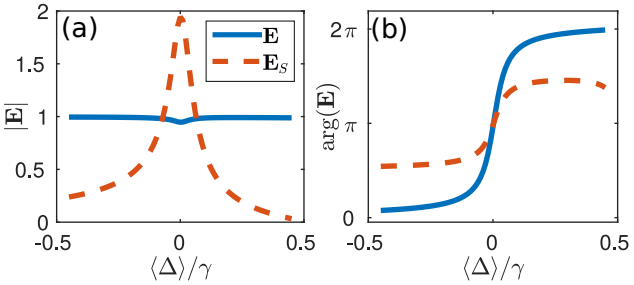

FIG. S3. (a) The magnitude and (b) the phase of the total transmitted light and the scattered light for the same parameters, as Fig. 3(a) in the main section.

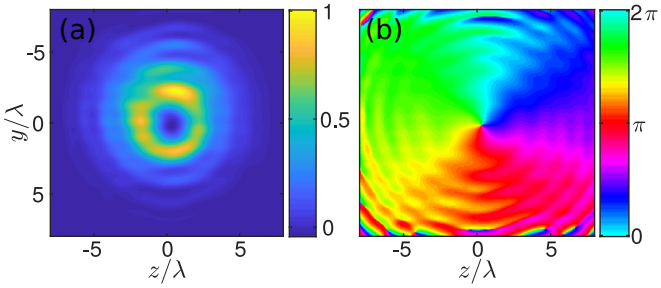

FIG. S4. (a) The transmitted intensity and (b) phase 5λ from a 20×20 Huygens' surface ($d = 0.8\lambda$, $a = 0.15\lambda$). An incident Gaussian beam with waist 5λ is transformed into an orbital angular momentum beam with angular $\hbar$ momentum per photon. Variations in the transmission are compensated by moving the center of the input beam a distance λ in the $-y$ direction.

electric and magnetic dipoles in a Huygens' surface add to give a scattered field with magnitude up to twice the incident field, as shown in Fig. S3(a), allowing for close to total transmission even when the scattered field is π out of phase with the incident light.

In the main text we demonstrate the Huygens' surface by transforming a Gaussian into a superposition of orbital angular momentum (OAM) states. The surface can also be used to create single OAM states, where $\mathbf{E} \propto \exp(il\phi)$ where ϕ is the azimuthal angle in the plane, with OAM $l\hbar$ per photon [S14]. The resulting intensity and phase is shown in Fig. S4 for $l = 1$, with a characteristic 2π phase winding around the center.

[S1] Stewart D. Jenkins and Janne Ruostekoski, "Controlled manipulation of light by cooperative response of atoms in an optical lattice," Phys. Rev. A **86**, 031602 (2012).

[S2] Mark D. Lee, Stewart D. Jenkins, and Janne Ruostekoski, "Stochastic methods for light propagation and recurrent scattering in saturated and nonsaturated atomic ensembles," Phys. Rev. A **93**, 063803 (2016).

[S3] John David Jackson, *Classical Electrodynamics*, 3rd ed. (Wiley, New York, 1999).

[S4] Anatoly A. Svidzinsky, Jun-Tao Chang, and Marlan O. Scully, "Cooperative spontaneous emission of n atoms: Many-body eigenstates, the effect of virtual Lamb shift processes, and analogy with radiation of n classical oscillators," Phys. Rev. A **81**, 053821 (2010).

[S5] S. D. Jenkins, J. Ruostekoski, J. Javanainen, S. Jennewein, R. Bourgain, J. Pellegrino, Y. R. P. Sortais, and A. Browaeys, "Collective resonance fluorescence in small and dense atom clouds: Comparison between theory and experiment," Phys. Rev. A **94**, 023842 (2016).

[S6] G. Facchinetti, S. D. Jenkins, and J. Ruostekoski, "Storing light with subradiant correlations in arrays of atoms," Phys. Rev. Lett. **117**, 243601 (2016).

[S7] B. Olmos, D. Yu, Y. Singh, F. Schreck, K. Bongs, and I. Lesanovsky, "Long-range interacting many-body systems with alkaline-earth-metal atoms," Phys. Rev. Lett. **110**, 143602 (2013).

[S8] Olaf Mandel, Markus Greiner, Artur Widera, Tim Rom, Theodor W. Hänsch, and Immanuel Bloch, "Controlled collisions for multi-particle entanglement of optically trapped atoms," Nature **425**, 937–940 (2003).

[S9] Michael Fleischhauer, Atac Imamoglu, and Jonathan P. Marangos, "Electromagnetically induced transparency: Optics in coherent media," Rev. Mod. Phys. **77**, 633–673 (2005).

[S10] L Chomaz, L Corman, T Yefsah, R Desbuquois, and J Dalibard, "Absorption imaging of a quasi-two-dimensional gas: a multiple scattering analysis," New Journal of Physics **14**, 055001 (2012).

[S11] Juha Javanainen, Janne Ruostekoski, Yi Li, and Sung-Mi Yoo, "Exact electrodynamics versus standard optics for a slab of cold dense gas," Phys. Rev. A **96**, 033835 (2017).

[S12] G. Facchinetti and J. Ruostekoski, "Interaction of light with planar lattices of atoms: Reflection, transmission, and cooperative magnetometry," Phys. Rev. A **97**, 023833 (2018).

[S13] Juha Javanainen and Renuka Rajapakse, "Light propagation in systems involving two-dimensional atomic lattices," Phys. Rev. A **100**, 013616 (2019).

[S14] L. Allen, S.M. Barnett, and M.J. Padgett, *Optical Angular Momentum*, Optics & Optoelectronics (Taylor & Francis, 2003).